RESEARCH ARTICLE | SEPTEMBER 05 2024

Impact of ultrathin garnet spacers on the magnetotransport in $Tb_3Fe_5O_{12}$/Pt bilayers

Pei Gen Li ; Sheung Mei Ng ; Xin Yuan ; Fu Xiang Zhang ; Hon Fai Wong ; Chi Wah Leung

Appl. Phys. Lett. 125, 102404 (2024)
https://doi.org/10.1063/5.0219796

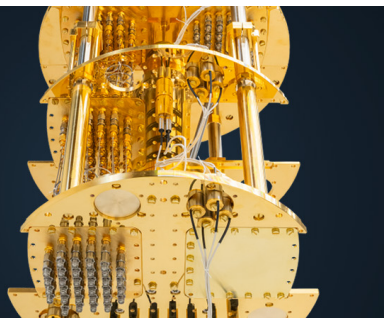

Applied Physics Letters
AIP Publishing

Applied Physics Letters ARTICLE pubs.aip.org/aip/apl

Impact of ultrathin garnet spacers on the magnetotransport in $Tb_3Fe_5O_{12}$/Pt bilayers

Cite as: Appl. Phys. Lett. **125**, 102404 (2024); doi: 10.1063/5.0219796
Submitted: 20 May 2024 · Accepted: 26 August 2024 ·
Published Online: 5 September 2024

Pei Gen Li,[1] Sheung Mei Ng,[1] Xin Yuan,[1,2] Fu Xiang Zhang,[2] Hon Fai Wong,[1] and Chi Wah Leung[1,a)]

AFFILIATIONS

[1]Department of Applied Physics, The Hong Kong Polytechnic University, Hung Hom, Hong Kong, China
[2]Songshan Lake Materials Laboratory, Dongguan, Guangdong 523808, China

[a)]Author to whom correspondence should be addressed: dennis.leung@polyu.edu.hk

ABSTRACT

We studied the interfacial spin Hall magnetotransport in the $Tb_3Fe_5O_{12}$ (TbIG)/Pt system across a non-magnetic [$Y_3Al_5O_{12}$ (YAG) and $Gd_3Ga_5O_{12}$ (GGG)] spacer with garnet structure. TbIG (30 nm)/spacer samples were grown on single-crystal (GGG) (111) substrates by pulsed laser deposition before 5 nm of Pt was sputtered on the samples and patterned into Hall bars. The YAG spacer thickness (t_{YAG}) dependences of anomalous Hall effect resistance (R_{AHE}) indicated no significant change on the magnetization compensation temperature of TbIG. Hysteretic R_{AHE} loops were observed at low magnetic fields, but with reducing magnitude as t_{YAG} thickness increases. A crossover of the R_{AHE} sign was observed at temperatures below the compensation temperature, which decreased sharply from 135 to 34 K as t_{YAG} increased from 0 to 1 nm. We attributed this to the strong dependence of the magnetic proximity effect toward the YAG insertion in the TbIG/Pt interface. Replacement of the YAG spacer with GGG showed significant impact on the R_{AHE} behavior. No obvious R_{AHE}-H loops were observed in the TbIG/Pt sample inserted with 0.5 nm GGG spacer, which could be linked to the strong magnetic contribution of the Gd ions. This work highlights the tunability of interfacial transport behavior in iron garnet/heavy metal systems through ultrathin spacers, providing guidance for the interfacial design of spintronic devices.

Ferrimagnetic insulator (FMI)/heavy metal (HM) devices play an important role in studying spin Hall magnetotransport behavior,[1–4] as the strong spin–orbit coupling of HM (like Pt) enables spin current within the layer to be reflected or absorbed by the FMI/HM interface and converted back into a charge current in the HM layer, achieving information transmission.[5,6] This spin transport is closely related to the FMI/HM interface, because two important interface effects, spin Hall effect (SHE) and magnetic proximity effect (MPE),[7] would affect the direction and intensity of spin current.

The peculiar interface effects have attracted the attention of researchers, with focus on spin current phenomena like spin pumping,[8,9] spin Seebeck effect,[10,11] spin Hall effect (SHE), and inverse spin Hall effect (ISHE).[7,12] They also explored the complex interface using x-ray magnetic circular dichroism (XMCD) or polarized neutron reflectometry (PNR) measurements, trying to distinguish the physical origin of such effects. To achieve regulation of these interface effects, interface engineering is an effective means that helps spintronics devices to achieve controllable information storage.[13]

Due to the strong spin–orbit coupling, Pt has been widely used in such studies of FMI/HM systems.[14,15] The most commonly studied system is $Y_3Fe_5O_{12}$ (YIG)/Pt, in which the anomalous Hall effect (AHE) phenomenon can be easily observed.[6,16,17] In a related rare-earth iron garnet (REIG) structure, $Tb_3Fe_5O_{12}$ (TbIG)/Pt has demonstrated two sign crossovers in AHE resistance (R_{AHE}) with decreasing temperatures.[18,19] The first sign reversal at higher temperature coincides with the magnetization compensation point (T_{comp}) of TbIG, at which the saturation magnetization temporarily vanishes.[18,20,21] The effect is attributed to antiferromagnetically coupled Tb and Fe ions in the material, which exhibit different temperature dependences of magnetization. Similar T_{comp} phenomenon was also observed in systems such as DyIG/Pt[22] and GdIG/Pt.[23,24]

The second sign reversal of R_{AHE} (denoted as T_1) is considered to arise from the competition between MPE-induced effects in the Pt layer and spin Hall magnetotransport at the REIG/Pt interface.[19,21,25,26] This low-temperature R_{AHE} sign reversal can possibly be regulated through modifications of the FMI/HM interface, for example, by dusting with a foreign material.[27]

For REIG/Pt heterostructures with two R_{AHE} sign crossover behaviors, previous studies have focused on regulating T_{comp};[28,29] and relatively little attention was paid to the modulation of T_1. Some

reports attempted to insert non-magnetic barriers (such as Cu and Si) at the REIG/Pt interface to modify MPE or SHE,[2,30] but there was no systematic exploration of T_1 regulation. Moreover, the long spin diffusion length of Cu could interfere with the normal spin diffusion of Pt. In addition, metal spacers are polycrystalline in nature and have a crystal structure that is dramatically different from that of REIG, resulting in increased uncertainty in interface regulation. Selection of appropriate materials that ensures uniform interface quality and controlling of T_1 is worth exploring.

In this work, we study the impact of lattice-matching, non-magnetic spacer on the R_{AHE} behavior of TbIG/Pt. $Y_3Al_5O_{12}$ (YAG) is a non-magnetic material with garnet structure and a lattice constant (12.003 Å)[31] close to that of TbIG (12.436 Å).[32] These conditions imply the possibility for coherent YAG growth on TbIG (particularly for ultrathin YAG layers in which stress relaxation is mild),[31,33] and therefore YAG was selected here as the spacer material. Meanwhile, another lattice-matching paramagnetic spacer of $Gd_3Ga_5O_{12}$ (GGG, lattice constant = 12.383 Å)[34] was also used for comparison. The lattice mismatch of TbIG/YAG is 3.48%, which is higher than that of TbIG/GGG (0.43%). In addition, previous works have confirmed that paramagnetic GGG can achieve spin transport like ferromagnetic insulators albeit with weaker signals.[35,36] The difference in magnetism between YAG and GGG could provide insights on the effect of different spacer layers on TbIG/Pt spin transport.

TbIG/YAG/Pt and TbIG/GGG/Pt samples were grown on GGG (111) substrates. The temperature (T) dependence of R_{AHE} in the samples for various spacer thicknesses was measured. T_{comp} was identified by a divergence of coercivity (H_c) in R_{AHE}-T plot, which coincides with the crossover of the R_{AHE} sign.[19] Within the YAG thickness (t_{YAG}) studied (1 nm or less), our results indicate no significant impact of the spacer on the measured T_{comp}, although the R_{AHE} amplitude decreases gradually. Below T_{comp}, a second R_{AHE} sign reversal is observed and is attributed to the competition between MPE-induced AHE and spin Hall (SH)-induced AHE. The ultrathin spacer strongly modulates the MPE behavior, and the presence of ultrathin spacers leads to a rapid decrease in this R_{AHE} sign reversal temperature. Apart from YAG, paramagnetic spacer of GGG also strongly inhibits the spin transport at the interface at even extremely thin cases (0.5 nm or less). Possible reasons for the observed differences are discussed.

TbIG (30 nm) with ultrathin YAG overlayers (thicknesses t_{YAG} between 0 and 2 nm) were deposited on GGG (111) single-crystal substrates by pulsed laser deposition, using a KrF laser (wavelength $\lambda = 248$ nm), in an oxygen ambient of 100 mTorr and substrate temperature of 710 °C. The substrates were pre-cleaned and pre-annealed in an oxygen environment of 1000 °C for 6 h, yielding a reconstructed surface that promotes the smooth growth of films.[18] The deposited films were post-annealed for 10 min at the same temperature *in situ* with 10 Torr oxygen pressure. Afterward, 5 nm of Pt was deposited on the samples by dc magnetron sputtering (base pressure better than 1×10^{-6} Torr) and patterned into Hall bars (channel size $100 \times 50\ \mu m^2$) by photolithography and Ar ion etching. Au (50 nm)/Ti (5 nm) electrodes were deposited by e-beam evaporation (pressure less than 1×10^{-6} Torr). The schematic of the completed device is shown in Fig. 1(a).

X-ray diffraction (XRD) measurements were conducted using a high-resolution x-ray diffractometer (Rigaku SmartLab) with Cu K_α ($\lambda = 1.541$ Å) radiation. Atomic force microscopy (AFM, Asylum 3D infinity) was used to characterize the surface morphology of the thin films. High-resolution transmission electron microscopy (HR-TEM) images were captured by spherical aberration-corrected transmission

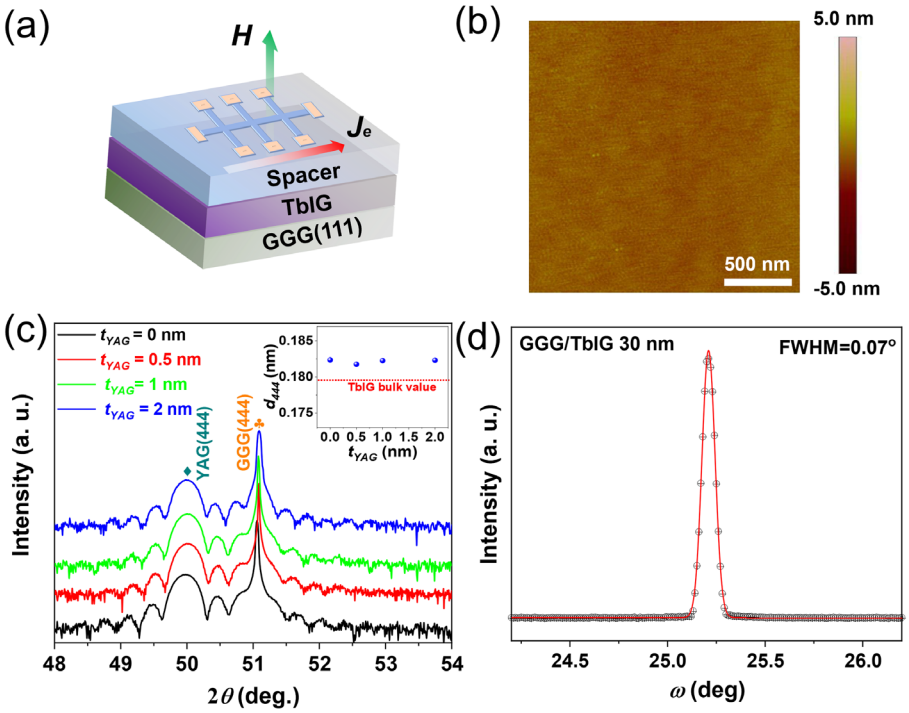

FIG. 1. (a) Schematic illustration of TbIG/spacer/Pt device for AHE measurements. J_e represents the electric current, and H is the external field. (b) AFM image of TbIG (30 nm) (scan area: $2 \times 2\ \mu m^2$). (c) XRD diffraction profile of TbIG (30 nm)/YAG bilayers with different YAG thicknesses. Inset: lattice spacing of TbIG (444) as a function of t_{YAG}. (d) Rocking curve of the TbIG (30 nm) sample.

electron microscope (AC-TEM) equipped with high-angle annular dark field (HAADF) and the energy-dispersive x-ray spectroscopy (EDX) to analyze the element distribution and atomic structure. R_{AHE}-H loops were measured using a physical property measurement system (PPMS, Quantum Design). Due the out-of-plane tensile stress and positive magnetostriction coefficient, TbIG deposited on GGG (111) exhibits perpendicular magnetic anisotropy (PMA).[18,37] The R_{AHE} was measured from the samples with a magnetic field applied normal to the sample surface.

Figure 1(b) presents the AFM scan of the TbIG (30 nm) sample, indicating an atomically smooth surface with a root mean square roughness of 0.21 nm. Figure 1(c) shows the θ-2θ scan of TbIG/YAG bilayer films for different t_{YAG} values. In addition to the sharp GGG (444) substrate peak, the TbIG film peak can be identified at smaller 2θ values. The extracted lattice spacing of $d_{444} = 0.182$ nm [inset of Fig. 1(c)] shows an out-of-plane expansion compared to the bulk value (0.1795 nm). With increasing t_{YAG}, the peak position of the bilayer films has shown a minute increase. Meanwhile, the ultrathin YAG layer is not expected to have a significant impact on the epitaxial growth of the underlying TbIG, as confirmed by the similar Laue oscillations and lattice spacing of the TbIG layer. The TbIG (444) peak rocking curve of the GGG/TbIG (30 nm) sample [Fig. 1(d)] shows a full-width at half-maximum (FWHM) of 0.07°, indicating a low mosaic spread. Samples with YAG overlayers essentially show the same FWHM.

A TbIG (30 nm)/YAG (2 nm)/Pt sample was prepared by focused ion beam (FIB) etching for HR-TEM. As shown in Fig. 2(a), the YAG layer can be clearly recognized through the cross-sectional TEM image. EDX mapping shows minute interdiffusion of each interface, which is a common phenomenon in garnet thin film systems.[38,39] HR-TEM [Figs. 2(b) and 2(c)] shows a coherent atomic arrangement of garnet structure along the $[11\bar{2}]$ direction for the TbIG/YAG. Although there is a lattice mismatch of 3.48% between TbIG and YAG, there is no significant lattice distortion observed in the YAG layer and good epitaxy is shown in the GGG/TbIG/YAG system. Line scan results in Fig. 2(d) indicate that the interdiffusion length is less than 0.5 nm across the TbIG/YAG interface. It provides evidence for comparing magnetotransport difference caused by direct and non-direct contact in TbIG/YAG/Pt systems.

The two crossover behavior in R_{AHE}-T plots of TbIG/Pt has been reported previously.[18,38] Although the interface coupling can affect the R_{AHE} signals, it remains to be explored whether changing interface coupling will affect the behavior of T_{comp} and T_1. Here, an ultrathin layer of non-magnetic YAG (from 0 to 2 nm) is inserted between Pt and TbIG to regulate the interface. Figure 3 compares the temperature-dependent R_{AHE} of TbIG/YAG/Pt samples with varying t_{YAG}. Several R_{AHE}-H loops present distortions at high field [e.g., Fig. 3(c)]. Similar AHE distortion has been observed in TmIG/Pt systems, which may be attributed to the nonlinear background signal contribution at high fields.[21,40] Such distortions should not affect the observation of AHE signal along the field sweeping direction.

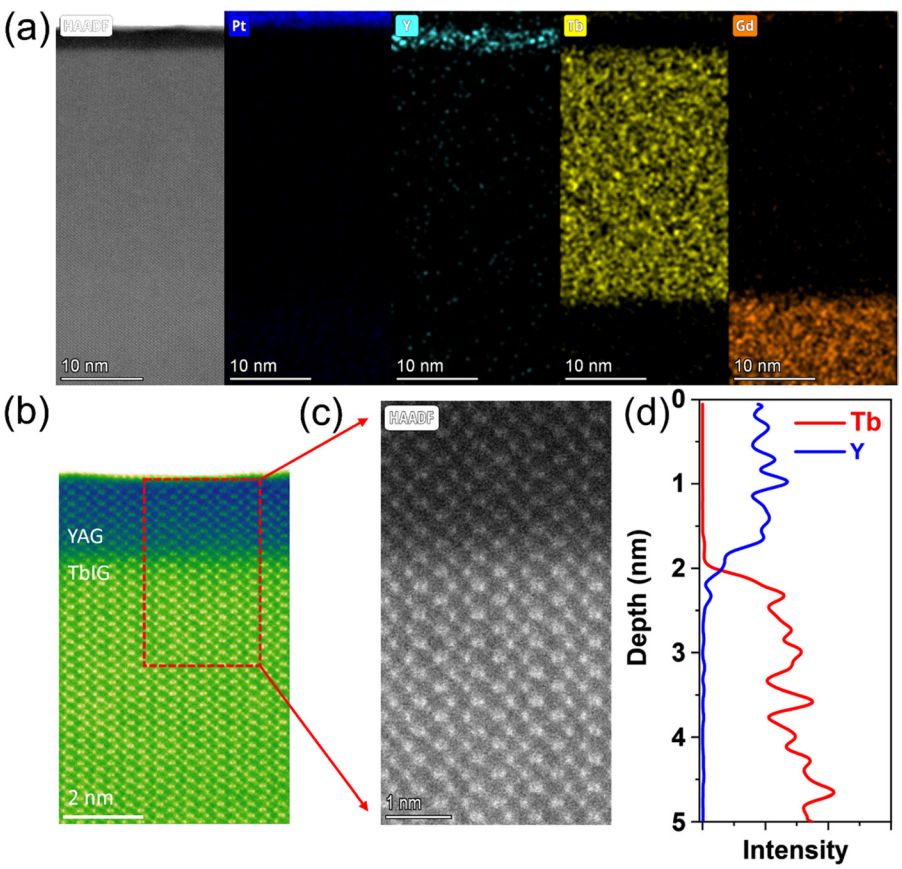

FIG. 2. (a) Cross-sectional TEM image of the TbIG/YAG (2 nm)/Pt sample. Element distribution of Gd, Tb, Y, and Pt are extracted from the EDX mapping. (b) HR-TEM image of the TbIG/YAG interface, with the magnified TbIG/YAG interface extracted from the enclosed range displayed in (c). (d) Average signal intensity of Tb and Y as obtained from the line scan in (c).

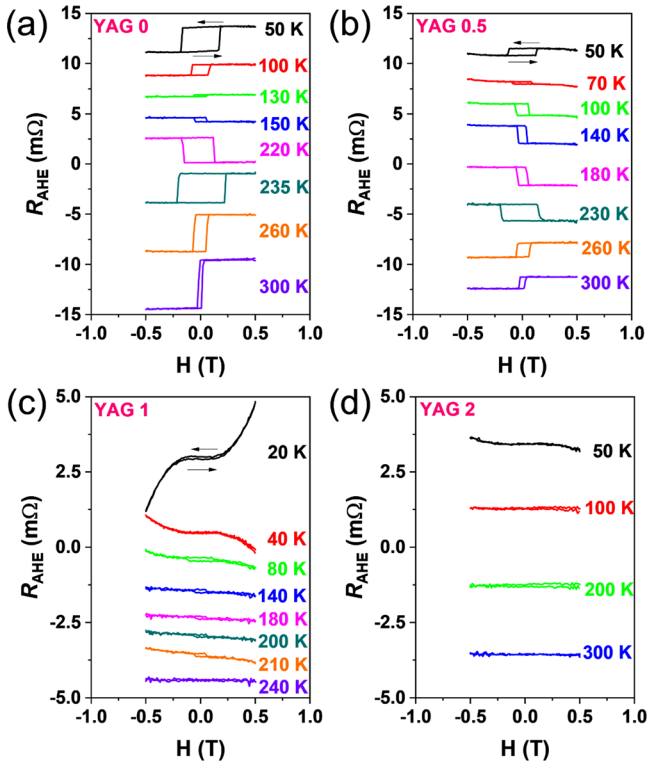

FIG. 3. Temperature-dependent R_{AHE}-H loops of TbIG (30 nm)/YAG/Pt, with $t_{YAG} = 0$ nm (a), 0.5 nm (b), 1 nm (c), and 2 nm (d). Black arrows indicate the scanning directions of the external magnetic field. In all plots, measurements at different temperatures are offset in the y-axis direction.

For the control sample [$t_{YAG} = 0$, Fig. 3(a)], as temperature decreases from 300 K, the first R_{AHE} sign change occurs at around 230 K. A similar R_{AHE} sign reversal behavior at around the same temperature is also observed in other samples with YAG spacers [Figs. 3(b) and 3(c)]. When the thickness of YAG increases to 2 nm [Fig. 3(d)], the AHE characteristics of TbIG cannot be discerned across the whole temperature range, indicating that 2 nm of YAG is sufficient to block the coupling between TbIG and Pt.

Apart from the sign reversal mentioned earlier, the samples also demonstrate a second R_{AHE} sign reversal at lower temperatures. For the control sample ($t_{YAG} = 0$), this occurs at around 135 K and is much higher than that of samples with YAG spacers (~65 K for $t_{YAG} = 0.5$ nm, below 34 K for $t_{YAG} = 1$ nm, and completely disappear for $t_{YAG} = 2$ nm).

To observe the variations in AHE more intuitively, temperature-dependent H_c and R_{AHE} at zero magnetic field (R^0_{AHE}) are extracted from R_{AHE}-H loops in Fig. 3 and are presented in Fig. 4, with H_c extracted from $R_{AHE} = 0$ at various temperatures. Due to the absence of AHE signal at $t_{YAG} = 2$ nm, the corresponding H_c and R_{AHE} cannot be obtained for comparison.

As shown in Figs. 4(a) and 4(b), a similar divergence of H_c takes place around 230 K in all samples, accompanied by a sudden sign reversal of R^0_{AHE}, indicating the occurrence of T_{comp}. Within the measurement error, we conclude that the YAG spacer layer does not change the temperature where H_c divergence occurs. The T_{comp} value is slightly lower than that of bulk value (about 246 K), possibly because of the strain state in the deposited TbIG layer.[41,42]

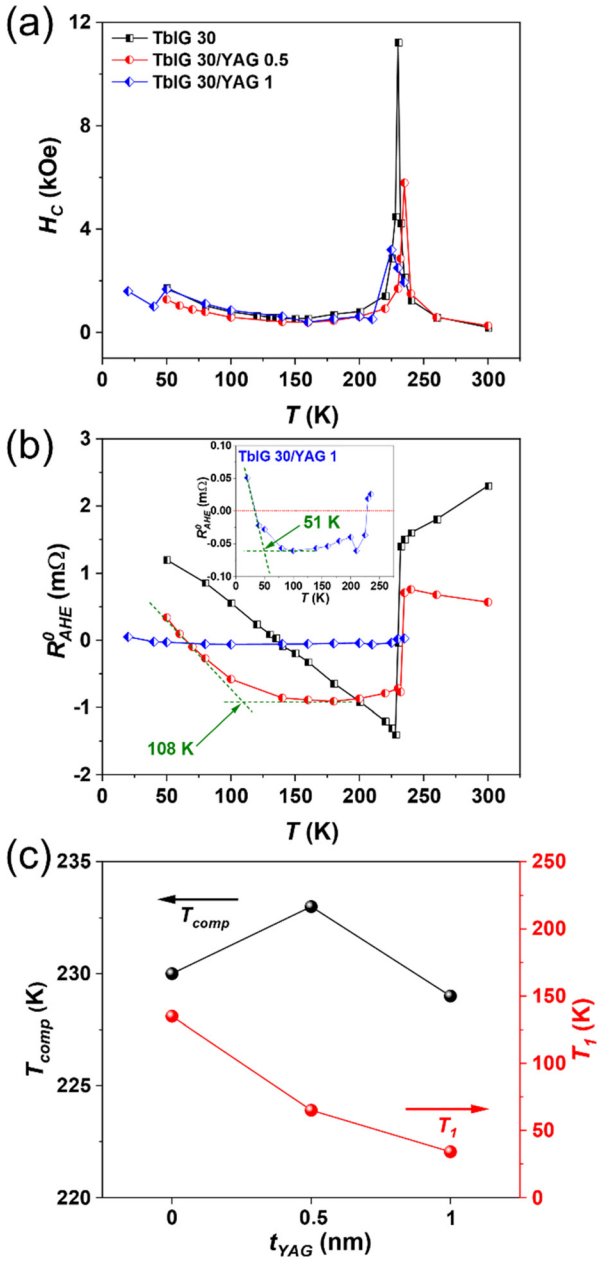

FIG. 4. Temperature dependence of (a) H_c and (b) R^0_{AHE} for different YAG thicknesses, as extracted from R_{AHE}-H loops in Fig. 3. Inset in (b) shows the enlarged $R^0_{AHE} - T$ curve for $t_{YAG} = 1$ nm sample. (c) Comparison of T_{comp} and T_1 for samples with different YAG thickness. Notice the difference of y-axes scales for T_{comp} (black) and T_1 (red) plots.

It is known that antiferromagnetic coupling exists between Fe^{3+} and Tb^{3+} ions in TbIG, which is the origin of its ferrimagnetic

behavior.[18] The temperature-dependent magnetizations of Tb^{3+} (at dodecahedral sites) and Fe^{3+} (at tetrahedral and octahedral sites) cancel out at T_{comp}. Similar behavior also occurs in other REIG like GdIG[43] and DyIG[22] and were probed with R_{AHE}.

Meanwhile, the interfacial exchange coupling of REIG/Pt is dominated by Fe/Pt exchange coupling,[21,22] with the R_{AHE} sign being determined by the Fe^{3+} moment orientation. At above T_{comp}, Fe^{3+} dominates the net magnetization of TbIG. As temperature decreases to T_{comp}, the moment of Fe^{3+} is wholly canceled out at T_{comp} by the Tb^{3+} moment (which has a more dramatic temperature dependence). Such a magnetization cancellation can be reflected through the divergent H_c. When the temperature continues to decrease, the decreased Zeeman energy would reorient the magnetic moments of Fe^{3+},[44] resulting in a sudden sign flip of R^0_{AHE}, reflected in R^0_{AHE} as a sharp sign reversal from positive to negative values [Fig. 4(b)].

Consistent divergence of H_c and sudden reversal of R^0_{AHE} sign behaviors across all TbIG/YAG/Pt samples (Fig. 4) indicate that the YAG spacer does not alter the antiferromagnetic coupling between the Fe^{3+} and Tb^{3+} in the TbIG layer, and confirms that the interface exchange coupling of TbIG/Pt is independent of T_{comp}.

At lower temperatures, the R^0_{AHE} sign reversal occurs again at T_1. The transition temperature T_1 varies drastically from ~135 K for the control sample to ~35 K for $t_{YAG} = 1$ nm. As mentioned earlier, the occurrence of T_1 is attributed to the competition between SHE and MPE.[19,21,25,26] For AHE induced by SHE, the spin-mixing conductance $G_{\uparrow\downarrow} = G_r + iG_i$ at the FMI/HM interface plays a great role in generating AHE.[3] According to Chen *et al.*,[45] the SHE-induced AHE needs to consider multiple factors, including (temperature dependent) conductivity σ, spin Hall angle θ_{SH}, spin diffusion length λ of Pt, and the spin-mixing conductance $G_{\uparrow\downarrow}$ at the TbIG/Pt interface. This leads to the attenuated SHE-induced AHE as temperature goes down. The other contribution of AHE originates from MPE, which leads to magnetic ordering in Pt and resulting in additional AHE signal. The MPE-induced AHE is strongly related to the exchange coupling between interfacial Fe^{3+} and Pt. The magnetic moment of Fe^{3+} is increased as the temperature goes down, and the Fe/Pt exchange coupling strength also increases accordingly, which leads to the MPE-induced AHE becoming stronger at low temperatures.

Unlike the R_{AHE} sign change around T_{comp}, no H_c divergence is observed at T_1, and the sign reversal process occurs more gradually with temperature. Reports have demonstrated a more dominant role of SHE on AHE at higher temperatures,[46] and MPE induced AHE dominates at low temperatures.[21,22] Considering the continuously increased MPE and decreased SHE as the temperature goes down, the crossover of R^0_{AHE} occurs at T_1 in TbIG/Pt.

It is worth noting that the R^0_{AHE} amplitude is reduced dramatically as the YAG thickness increases. As shown in Fig. 4(b), the R_{AHE} amplitude decays exponentially from 1.5 mΩ (for $t_{YAG} = 0$) to virtually zero (for $t_{YAG} = 2$ nm) at 235 K. The magnetic ordering in Pt induced by MPE occurs in the region very close to the TbIG/Pt interface, and SHE also depends on the spin accumulation at the TbIG/Pt interface. After the insertion of non-magnetic YAG, the coupling of Fe/Pt will be severely weakened, and the magnetic ordering within Pt is highly dependent on direct contact with TbIG, which means that the competitive balance between MPE and SHE would be disrupted, and the induced AHE signals would be weakened, displayed as a decreased R^0_{AHE} amplitude.

The slope of R^0_{AHE} plots also provide some insight on the temperature dependence of MPE and SHE. As shown in Fig. 4(b), the R^0_{AHE} plot of the control sample ($t_{YAG} = 0$ nm) exhibits a constant slope between T_{comp} and T_1, indicating that the competitive balance between MPE and SHE follows a linear variation. Based on the competitive relationship between MPE and SHE, and the fact that MPE dominates at low temperatures,[21,22] we speculate that rising MPE impact in AHE from T_{comp} onward with decreasing temperature.

With YAG intervention, it is noticed that such a linear variation of the R^0_{AHE} at low temperatures occurs in an increasingly narrow temperature range with rising t_{YAG} values. Instead, the plots retain a fair steady amplitude for temperatures between T_{comp} and T_1. Assuming the MPE impact takes effect at a transition temperature such that the R^0_{AHE} plot slope changes [see Fig. 4(b) for details], such transition occurs at ~108 K for $t_{YAG} = 0.5$ nm and ~51 K for $t_{YAG} = 1$ nm. This indicates that the YAG spacer has a greater impact on the temperature dependence of MPE, with MPE-induced AHE becoming more suppressed as t_{YAG} increases.

Figure 5 shows the normalized R^0_{AHE} with an evident exponential decay with t_{YAG} increases. The fitting curve follows the formula $\frac{R^0_{AHE}}{R^0_{AHE}(t_{YAG}=0)} = e^{-t_{YAG}/\lambda}$, where λ is the decay length. A decay length of $\lambda = 0.26$ nm across the YAG spacer was obtained.

Considering that the TbIG and Pt are separated by the insulating YAG spacer, it is speculated that the coupling between TbIG and Pt originates from the quantum tunneling across the barrier; similar effect has been observed in YIG systems.[30,47] The ability of spin-polarized electrons in Pt to pass through spacer barriers can be evaluated by the spin tunneling transmission coefficient D_{ttc}. This is strongly correlated with the Schottky barrier $\emptyset_{sc}$ and spacer thickness t and is described as $D_{ttc} \propto \exp\left[\frac{-2t_{YAG}\sqrt{2m\emptyset_{sc}}}{\hbar}\right]$,[30] where m and $\hbar$ represent the effective electron mass and Planck's constant. This indicates that the spin transport achieved by tunneling is negatively correlated with the thickness and work function of the spacer.

To explore the universality of the simple barrier model, we chose another paramagnetic garnet GGG as the spacer layer. The commonality between GGG and YAG is the similar garnet structure with TbIG,

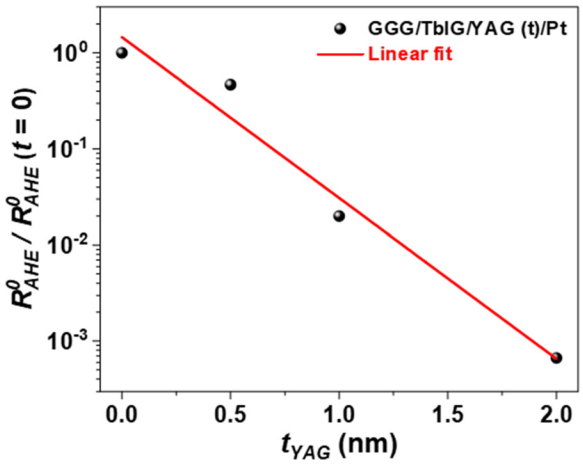

FIG. 5. Semi-log plots of normalized R^0_{AHE} as a function of the YAG thickness at 235 K. The fit indicates a decay length $\lambda = 0.26$ nm in the TbIG/YAG/Pt system.

which can ensure the uniform crystallinity of the spacer layer and similar interface quality. However, GGG demonstrates strong paramagnetism, while YAG is largely non-magnetic. The strong magnetic moment of Gd^{3+} in GGG under Curie temperature (292 K)[48] may alter the magnetotransport dominated by TbIG. This allows us to explore the difference between non-magnetic and paramagnetic garnet as spacer.

As shown in Fig. 6, samples inserted with 0.5 and 1 nm GGG spacer exhibit almost identical R_{AHE}-H signals, with no AHE loop to be observed. It can be considered that only the signal of the GGG spacer is displayed, indicating a strong attenuation of tunneling with just 0.5 nm of GGG spacer. Considering YAG and GGG spacers of the same thickness by the barrier model mentioned earlier (the Schottky barrier $\emptyset_{sc}$ is expected to be half of the spacer bandgap[30]) with bandgap of YAG being 6.5 eV[49] and is higher than that of GGG (5.66 eV).[50] Theoretically, the larger bandgap means lower ability of tunneling. However, comparing the results of 0.5 nm spacers in Figs. 3(b) and 6(a), it is evident that the decay length in the YAG spacer is much larger than that in the GGG spacer. This indicates that in addition to the barrier model, other factors need to be considered to judge the ability of tunneling. Although it is known that the spin transport is achieved in FMI through the propagation of magnon,[51] one should consider the strong paramagnetism of GGG, the 4*f*-shell of Gd^{3+} contributes a large local moment,[52] which could significantly attenuate the spin transport from TbIG to Pt layer.

In summary, magnetotransport at the TbIG/Pt interface with non-magnetic YAG and paramagnetic GGG spacer layer was studied. T_{comp} of TbIG/Pt remained at ~230 K with varied YAG spacer thicknesses, indicating that the interface exchange coupling of TbIG/Pt is independent of T_{comp}. On the other hand, the presence of YAG spacer significantly affected the interfacial competition between MPE and SHE, leading to an exponential drop of R^0_{AHE} amplitude. The second crossover of R_{AHE} sign T_1 dropped significantly from ~135 K for the control sample to ~35 K for $t_{YAG} = 1$ nm, indicating the controllability of T_1. Finally, paramagnetic GGG spacer exhibited stronger attenuation of R_{AHE} signals than non-magnetic YAG, which was attributed to strong Gd^{3+} magnetic moment. The study illustrates the impact of spacer and interface on the AHE switching behavior, which would be helpful for the engineering of FMI/HM heterostructures and interfaces for spintronic applications.

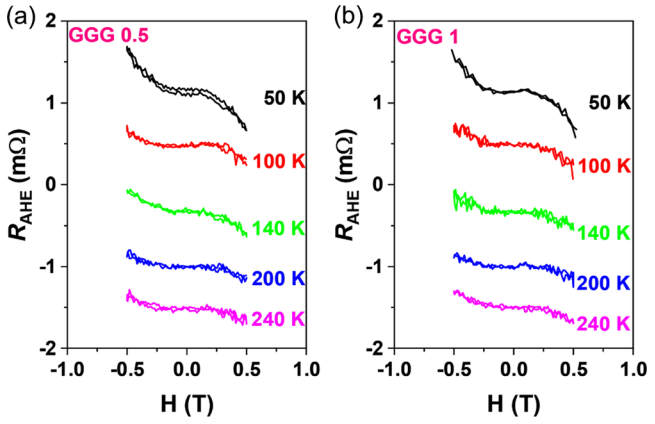

FIG. 6. Temperature-dependent R_{AHE}-H loops of TbIG (30 nm)/GGG/Pt, with $t_{GGG} = 0$ nm (a), 0.5 nm (b).

The work was supported by the Research Grants Council, HKSAR (No. 15302320), and the Hong Kong Polytechnic University (ZVWC).

AUTHOR DECLARATIONS

Conflict of Interest

The authors have no conflicts to disclose.

Author Contributions

Pei Gen Li: Conceptualization (supporting); Data curation (lead); Formal analysis (lead); Investigation (lead); Methodology (lead); Writing – original draft (lead). **Sheung Mei Ng:** Investigation (supporting); Methodology (supporting); Writing – review & editing (supporting). **Xin Yuan:** Investigation (supporting); Methodology (supporting); Writing – review & editing (supporting). **Fu Xiang Zhang:** Investigation (supporting); Methodology (supporting); Writing – review & editing (supporting). **Hon Fai Wong:** Investigation (supporting); Methodology (supporting); Writing – review & editing (supporting). **Chi Wah Leung:** Conceptualization (lead); Formal analysis (lead); Funding acquisition (lead); Project administration (lead); Resources (lead); Supervision (lead); Writing – review & editing (equal).

DATA AVAILABILITY

The data that support the findings of this study are available from the corresponding author upon reasonable request.

REFERENCES

[1]S. Meyer, M. Althammer, S. Geprägs, M. Opel, R. Gross, and S. T. B. Goennenwein, Appl. Phys. Lett. **104**(24), 242411 (2014).
[2]C. Tang, P. Sellappan, Y. Liu, Y. Xu, J. E. Garay, and J. Shi, Phys. Rev. B **94**(14), 140403 (2016).
[3]S. Meyer, R. Schlitz, S. Geprägs, M. Opel, H. Huebl, R. Gross, and S. T. B. Goennenwein, Appl. Phys. Lett. **106**(13), 132402 (2015).
[4]S. Shimizu, K. S. Takahashi, T. Hatano, M. Kawasaki, Y. Tokura, and Y. Iwasa, Phys. Rev. Lett. **111**(21), 216803 (2013).
[5]J. Sinova, S. O. Valenzuela, J. Wunderlich, C. H. Back, and T. Jungwirth, Rev. Mod. Phys. **87**(4), 1213 (2015).
[6]M. Althammer, S. Meyer, H. Nakayama, M. Schreier, S. Altmannshofer, M. Weiler, H. Huebl, S. Geprägs, M. Opel, R. Gross, D. Meier, C. Klewe, T. Kuschel, J.-M. Schmalhorst, G. Reiss, L. Shen, A. Gupta, Y.-T. Chen, G. E. W. Bauer, E. Saitoh, and S. T. B. Goennenwein, Phys. Rev. B **87**(22), 224401 (2013).
[7]H. Nakayama, M. Althammer, Y. T. Chen, K. Uchida, Y. Kajiwara, D. Kikuchi, T. Ohtani, S. Geprags, M. Opel, S. Takahashi, R. Gross, G. E. Bauer, S. T. Goennenwein, and E. Saitoh, Phys. Rev. Lett. **110**(20), 206601 (2013).
[8]M. V. Costache, M. Sladkov, S. M. Watts, C. H. van der Wal, and B. J. van Wees, Phys. Rev. Lett. **97**(21), 216603 (2006).
[9]O. Mosendz, J. E. Pearson, F. Y. Fradin, G. E. Bauer, S. D. Bader, and A. Hoffmann, Phys. Rev. Lett. **104**(4), 046601 (2010).
[10]S. M. Wu, W. Zhang, A. Kc, P. Borisov, J. E. Pearson, J. S. Jiang, D. Lederman, A. Hoffmann, and A. Bhattacharya, Phys. Rev. Lett. **116**(9), 097204 (2016).
[11]Z. Jiang, C. Z. Chang, M. R. Masir, C. Tang, Y. Xu, J. S. Moodera, A. H. MacDonald, and J. Shi, Nat. Commun. **7**, 11458 (2016).
[12]B. F. Miao, S. Y. Huang, D. Qu, and C. L. Chien, Phys. Rev. Lett. **111**(6), 066602 (2013).

[13]S. Jiang, X. Chen, X. Li, K. Yang, J. Zhang, G. Yang, Y. Liu, J. Lu, D. Wang, J. Teng, and G. Yu, Appl. Phys. Lett. **107**(11), 112404 (2015).
[14]P. Blonski, S. Dennler, and J. Hafner, J. Chem. Phys. **134**(3), 034107 (2011).
[15]P. M. Haney, H.-W. Lee, K.-J. Lee, A. Manchon, and M. D. Stiles, Phys. Rev. B **87**(17), 174411 (2013).
[16]H. L. Wang, C. H. Du, Y. Pu, R. Adur, P. C. Hammel, and F. Y. Yang, Phys. Rev. Lett. **112**(19), 197201 (2014).
[17]Y. K. Liu, H. F. Wong, X. Guo, S. M. Ng, K. K. Lam, Y. Zhu, C. L. Mak, and C. W. Leung, ACS Appl. Electron. Mater. **1**(7), 1099 (2019).
[18]Y. K. Liu, H. F. Wong, K. K. Lam, K. H. Chan, C. L. Mak, and C. W. Leung, J. Magn. Magn. Mater. **468**, 235 (2018).
[19]P. G. Li, J. M. Liang, S. M. Ng, H. F. Wong, Y. Zhou, L. J. Huang, K. W. Lin, Y. H. Tsang, C. L. Mak, and C. W. Leung, J. Magn. Magn. Mater. **592**, 171785 (2024).
[20]S. Becker, Z. Ren, F. Fuhrmann, A. Ross, S. Lord, S. Ding, R. Wu, J. Yang, J. Miao, M. Kläui, and G. Jakob, Phys. Rev. Appl. **16**(1), 014047 (2021).
[21]Q. Shao, A. Grutter, Y. Liu, G. Yu, C.-Y. Yang, D. A. Gilbert, E. Arenholz, P. Shafer, X. Che, C. Tang, M. Aldosary, A. Navabi, Q. L. He, B. J. Kirby, J. Shi, and K. L. Wang, Phys. Rev. B **99**(10), 104401 (2019).
[22]J. J. Bauer, P. Quarterman, A. J. Grutter, B. Khurana, S. Kundu, K. Andre Mkhoyan, J. A. Borchers, and C. A. Ross, Phys. Rev. B **104**(9), 094403 (2021).
[23]B. W. Dong, J. Cramer, K. Ganzhorn, H. Y. Yuan, E. J. Guo, S. T. B. Goennenwein, and M. Klaui, J. Phys.: Condens. Matter **30**(3), 035802 (2018).
[24]L. Liu, Z. Fan, Z. Chen, Z. Chen, Z. Ye, H. Zheng, Q. Zeng, W. Jia, S. Li, N. Wang, J. Liu, L. Ma, T. Lin, M. Qiu, S. Li, P. Han, J. Shi, and H. An, Appl. Phys. Lett. **119**(5), 052401 (2021).
[25]W. Zhang, M. B. Jungfleisch, W. Jiang, Y. Liu, J. E. Pearson, S. G. E. Te Velthuis, A. Hoffmann, F. Freimuth, and Y. Mokrousov, Phys. Rev. B **91**(11), 115316 (2015).
[26]S. Ding, Z. Liang, C. Yun, R. Wu, M. Xue, Z. Lin, A. Ross, S. Becker, W. Yang, X. Ma, D. Chen, K. Sun, G. Jakob, M. Kläui, and J. Yang, Phys. Rev. B **104**(22), 224410 (2021).
[27]W. Amamou, I. V. Pinchuk, A. H. Trout, R. E. A. Williams, N. Antolin, A. Goad, D. J. O'Hara, A. S. Ahmed, W. Windl, D. W. McComb, and R. K. Kawakami, Phys. Rev. Mater. **2**(1), 011401 (2018).
[28]J. M. Liang, X. W. Zhao, Y. K. Liu, P. G. Li, S. M. Ng, H. F. Wong, W. F. Cheng, Y. Zhou, J. Y. Dai, C. L. Mak, and C. W. Leung, Appl. Phys. Lett. **122**(24), 242401 (2023).
[29]Y. F. Li, X. H. Yang, H. Bai, M. Z. Wang, D. S. Cheng, C. Song, Z. Yuan, Y. Liu, and Z. Shi, Phys. Rev. B **108**(18), 184403 (2023).
[30]C. H. Du, H. L. Wang, Y. Pu, T. L. Meyer, P. M. Woodward, F. Y. Yang, and P. C. Hammel, Phys. Rev. Lett. **111**(24), 247202 (2013).
[31]Y. K. Liu, J. M. Liang, H. F. Wong, S. M. Ng, C. L. Mak, and C. W. Leung, J. Magn. Magn. Mater. **536**, 168130 (2021).
[32]H. Fuess, G. Bassi, M. Bonnet, and A. Delapalme, Solid State Commun. **18**(5), 557 (1976).
[33]J. M. Liang, X. W. Zhao, S. M. Ng, H. F. Wong, Y. K. Liu, C. L. Mak, and C. W. Leung, IEEE Trans. Magn. **58**(2), 1 (2022).
[34]S. Mokarian Zanjani, M. C. Onbaşlı, and J. Magn, Magn. Mater. **499**, 166108 (2020).
[35]S. M. Wu, J. E. Pearson, and A. Bhattacharya, Phys. Rev. Lett. **114**(18), 186602 (2015).
[36]K. Oyanagi, S. Takahashi, L. J. Cornelissen, J. Shan, S. Daimon, T. Kikkawa, G. E. W. Bauer, B. J. van Wees, and E. Saitoh, Nat. Commun. **10**(1), 4740 (2019).
[37]V. H. Ortiz, M. Aldosary, J. Li, Y. Xu, M. I. Lohmann, P. Sellappan, Y. Kodera, J. E. Garay, and J. Shi, APL Mater. **6**(12), 121113 (2018).
[38]R. Yadav, A. Bake, W. T. Lee, Y.-K. Liu, D. R. G. Mitchell, X.-R. Yang, D. L. Cortie, K.-W. Lin, and C. W. Leung, Phys. Rev. Mater. **7**(12), 124407 (2023).
[39]A. Mitra, O. Cespedes, Q. Ramasse, M. Ali, S. Marmion, M. Ward, R. M. D. Brydson, C. J. Kinane, J. F. K. Cooper, S. Langridge, and B. J. Hickey, Sci. Rep. **7**(1), 11774 (2017).
[40]C. N. Wu, C. C. Tseng, Y. T. Fanchiang, C. K. Cheng, K. Y. Lin, S. L. Yeh, S. R. Yang, C. T. Wu, T. Liu, M. Wu, M. Hong, and J. Kwo, Sci. Rep. **8**(1), 11087 (2018).
[41]S. Geller, J. P. Remeika, R. C. Sherwood, H. J. Williams, and G. P. Espinosa, Phys. Rev. **137**(3A), A1034 (1965).
[42]P. Wang, J. Ke, G. S. Li, L. Z. Bi, C. Hu, Z. Zhu, J. Liu, Y. Zhang, and J. W. Cai, Appl. Phys. Lett. **124**(17), 172405 (2024).
[43]Y. Li, D. Zheng, C. Liu, C. Zhang, B. Fang, A. Chen, Y. Ma, A. Manchon, and X. Zhang, ACS Nano **16**, 8181 (2022).
[44]K. J. Kim, S. K. Kim, Y. Hirata, S. H. Oh, T. Tono, D. H. Kim, T. Okuno, W. S. Ham, S. Kim, G. Go, Y. Tserkovnyak, A. Tsukamoto, T. Moriyama, K. J. Lee, and T. Ono, Nat. Mater. **16**(12), 1187 (2017).
[45]Y.-T. Chen, S. Takahashi, H. Nakayama, M. Althammer, S. T. B. Goennenwein, E. Saitoh, and G. E. W. Bauer, Phys. Rev. B **87**(14), 144411 (2013).
[46]E. R. Rosenberg, L. Beran, C. O. Avci, C. Zeledon, B. Song, C. G. Fuentes, J. Mendil, P. Gambardella, M. Veis, C. Garcia, G. S. D. Beach, and C. A. Ross, Phys. Rev. Mater. **2**(9), 094405 (2018).
[47]W. Chen, M. Sigrist, and D. Manske, Phys. Rev. B **94**(10), 104412 (2016).
[48]S. M. Benford and G. V. Brown, J. Appl. Phys. **52**(3), 2110 (1981).
[49]A. Kumar, R. Kumar, N. Verma, A. V. Anupama, H. K. Choudhary, R. Philip, and B. Sahoo, Opt. Mater. **108**, 110163 (2020).
[50]K. Ghimire, H. F. Haneef, R. W. Collins, and N. J. Podraza, Phys. Status Solidi B **252**(10), 2191 (2015).
[51]Q. Shao, C. Tang, G. Yu, A. Navabi, H. Wu, C. He, J. Li, P. Upadhyaya, P. Zhang, S. A. Razavi, Q. L. He, Y. Liu, P. Yang, S. K. Kim, C. Zheng, Y. Liu, L. Pan, R. K. Lake, X. Han, Y. Tserkovnyak, J. Shi, and K. L. Wang, Nat. Commun. **9**(1), 3612 (2018).
[52]M. J. Roos, P. Quarterman, J. Ding, M. Wu, B. J. Kirby, and B. L. Zink, Phys. Rev. Mater. **6**(3), 034401 (2022).